Preprints (www.preprints.org) | NOT PEER-REVIEWED | Posted: 9 July 2021 doi:10.20944/preprints202107.0212.v1

Article

Cell Stress Induces Mislocalization of Transcription Factors with Mitochondrial Enrichment

Chiara Rossi[1], Anna Fernàndez[1], Pascual Torres[1], Omar Ramirez-Nuñez[1], Ana Belén Granado-Serrano[1], Mònica Povedano[2], Reinald Pamplona[1], Isidro Ferrer[3,4,5,6,7], and Manuel Portero-Otin [1,*]

[1] Metabolic Physiopathology Research Group, Experimental Medicine Department, Lleida University-Lleida Biochemical Research Institute (UdL-IRBLleida], Lleida, Spain; clara70289@mex.udl.cat (C.R.]; anna.fernandez@udl.cat (A.F.]; pascual.torres@udl.cat (P.T.]; omar.ramirez78@gmail.com (O.R.-N.]; anabgs@mex.udl.cat (A.G-S.]; reinald.pamplona@udl.cat (R.P.]

[2] Functional Unit of Amyotrophic Lateral Sclerosis (UFELA], Service of Neurology, Bellvitge University Hospital, L'Hospitalet de Llobregat, Barcelona, Spain.; 30058mpp@gmail.com (M.P.] 9 10. 11 Department of Neurology, Columbia University Irving Medical Center, New York, NY, USA. 12 13 [3] Department of Pathology and Experimental Therapeutics, University of Barcelona, Barcelona, Spain

[4] CIBERNED (Network Centre of Biomedical Research of Neurodegenerative Diseases], Institute of Health Carlos III, Ministry of Economy and Competitiveness, Barcelona, Spain.

[5] Bellvitge Biomedical Research Institute (IDIBELL], Hospitalet de Llobregat, Barcelona, Spain

[6] Senior Consultant, Bellvitge University Hospital, Barcelona, Spain.

[7] Institute of Neurosciences, University of Barcelona, Barcelona, Spain; 8082ifa@gmail.com (I.F.]

* Correspondence: manuel.portero@udl.cat ; Tel.: (+34973702408], Edifici Biomedicina I, Avda Rovira Roure, 80 E25196 Lleida, Spain

Abstract Previous evidence links the formation of extranuclear inclusions of transcription factors, such as ERK, Jun, TDP-43, and REST with oxidative, endoplasmic-reticulum, proteasomal, and osmotic stress. To further characterize its extranuclear location, we performed a high-content screening based on confocal microscopy and automatized image analyses of an epithelial cell culture treated with hydrogen peroxide, thapsigargin, epoxomicin, or sorbitol at different concentrations and times to recreate the stresses mentioned above. We also performed subcellular fractionation of the brain from transgenic mice overexpressing the Q331K mutated TARDBP, and we analyzed REST-regulated mRNAs. The results show that these nuclear proteins exhibit a mitochondrial location, together with significant nuclear/extranuclear ratio changes, in a protein and stress-specific manner. The presence of these proteins in enriched mitochondrial fractions in vivo confirmed the results of image analyses. TDP-43 aggregation was associated with alteration in mRNA levels of REST target genes involved in calcium homeostasis, apoptosis, and metabolism. In conclusion, cell stress increased mitochondrial translocation of nuclear proteins, increasing the chance of proteostasis alterations. Further, TDP-43 aggregation impacts REST target genes, disclosing an exciting interaction between these two transcription factors in neurodegenerative processes.

Keywords: TDP-43; Jun; REST; ERK; mitochondria; cell stress; aggregation; transcription factors; transgenic mice; subcellular fractionation

1. Introduction

The presence of protein aggregates is a pathological hallmark for several neurodegenerative diseases, including Alzheimer's disease (AD), Parkinson's disease, and amyotrophic lateral sclerosis (ALS), to name a few[1] These protein aggregates show disease specificity. For instance, beta-amyloid aggregates characterize the AD neurofibrillary tangles and intracellular aggregates. Similarly, aggregates of highly phosphorylated TDP-43 are present in the cytosol of remaining motor neurons in ALS. Whether (and how) these aggregates are mere bystanders of ongoing pathogenic processes or whether they constitute bona fide cellular noxa is still under debate.

© 2021 by the author(s). Distributed under a Creative Commons CC BY license.

Preprints (www.preprints.org) | NOT PEER-REVIEWED | Posted: 9 July 2021 doi:10.20944/preprints202107.0212.v1

In the case of ALS, TDP-43 is a primary component of these aggregates. TDP-43 is a ubiquitous protein that belongs to the heterogeneous nuclear ribonucleoprotein family and is encoded by the TARDBP gene. TDP-43 is mainly found in the nucleus of normal cells and is involved in RNA regulation, including transcriptional regulation, alternative splicing, and mRNA stabilization [2]. TDP-43 is usually found in the nucleus, but it also moves between the nucleus and the cytoplasm to perform various cellular tasks. TDP-43's level and localization are tightly controlled by a negative feedback mechanism [3]. Under stress circumstances such as heat shock, oxidative stress, and arsenite exposure, nuclear TDP-43 is transferred to the cytoplasm, and cytoplasmic TDP-43 accumulates to form stress granules a variety of other proteins and RNAs[4]. When the stress is relieved, the SGs that carry TDP-43 break down, and TDP-43 released from the SGs translocates into the nucleus [5]. On the other hand, chronic stress causes extended SG formation, which leads to cytoplasmic TDP-43 aggregate accumulation.

In addition to TDP-43, other proteins with roles as transcriptional factors also show their cytoplasmic accumulation as aggregates [6]. We include p-ERK [7]and p-Jun[8]. Protein aggregation have been found in several neurodegenerative conditions, such as AD. Interestingly, recent data demonstrate that another protein, namely REST, could show decreased values during AD pathogenesis[9]. Similarly, REST is found as aggregates in the substantia nigra from PD patients[10]. In this context, it is known that cellular stress, such as ER, proteasome, or oxidative stress, can induce TDP-43 mislocalization[7].

Dysfunction of the nuclear pore complex is linked to cytoplasmic mislocalization and TDP-43 aggregation, in addition to dysregulation of stress granule formation[11]. Indeed one of the most common causes of ALS, associated with G4C2 repeats within the C9ORF72 gene, impairs the cytoplasm–nucleus gradient of Ran, the primary regulator of TDP-43 nuclear localization, according to several studies[12]. The structure of the nuclear membrane is similarly disrupted by (G4C2) RNA. TDP-43 is also linked to the cytoplasmic accumulation of other nuclear membrane proteins like Nup62 and Kpnb1[13]. Of note, we have recently demonstrated that ALS is associated with an alteration in the nuclear envelope lipids [14]

Besides p-TDP-43, p-ERK[7] and REST[10] also show aggregates in neurodegenerative diseases. Several authors have reported that TDP-43 protein aggregates may be found in organullar fractions in addition to the cytosolic location, such as mitochondria[15,16]. How cell stress is linked to this mislocalization is currently unknown, but it may include impairments in proteostasis and imbalances in autophagy flux[17]. To shed light on this question, we have explored if oxidative, ER and proteasome stress can induce changes in the cellular distribution of these transcription factors. Specifically, we focused on the potential interaction with mitochondria due to the relevance of mitochondrial (dys)function in neurodegenerative conditions (particularly in ALS). We validated the in vitro data by exploring the presence of these proteins in enriched mitochondrial fractions. Our results demonstrate that the interaction of TDP-43, REST, Jun, and ERK with extranuclear components, such as mitochondria, is dependent on cell stress. Further, we demonstrate an unreported association of TDP-43 pathology and changes in REST-dependent mRNAs. All in all, the enhanced mitochondrial interaction of these proteins could contribute to the reported loss of mitochondrial functions in several neurodegenerative processes.

2. Results

Oxidative stress induced by H2O2 in HMEC cells led to the accumulation of p-TDP-43, mainly in a cytoplasmic location, while the nuclear intensity of p-TDP-43 was preserved (Figure 1A). In contrast, despite an initial increase in a p-ERK cytosolic area in the same conditions, this protein was rapidly cleared (Figure 1A), being mainly non-nuclear. Cytoplasmic staining of p-Jun and REST showed the same tendencies, i.e., after

Preprints (www.preprints.org) | NOT PEER-REVIEWED | Posted: 9 July 2021 doi:10.20944/preprints202107.0212.v1

an initial decrease, there was a tendency for increasing their values (highly significant in the case of REST), as indicated in Figure 1A. Non-homogeneous distribution of cytoplasmic location after oxidative stress (evident in p-TDP-43, p-Jun, and REST) suggested its colocalization with an organelle fraction. We performed coimmunostaining with several mitochondrial epitopes to test if this non-nuclear localization involved a mitochondrial residence (as previously indicated in [18]). Complex V coimmunostaining with these factors (Figure 1B) indicated that the degree of colocalization increased significantly in all cases after oxidative stress, exceeding z' values of 0.5 (roughly meaning that at least 50% of both epitopes could coincide at the resolution of the confocal microscopy), except for p-ERK. Although the colocalization of this protein increased significantly after oxidative stress (Figure 1B), and in line with p-ERK decreased values in the cytoplasm, z' values did not reach 0.3 in this case. Correlation analyses of nuclear vs. cytoplasmic intensity showed linear relationships between these parameters, though their response to oxidative stress was strongly dependent on the factor (Supplemental Figure 1).

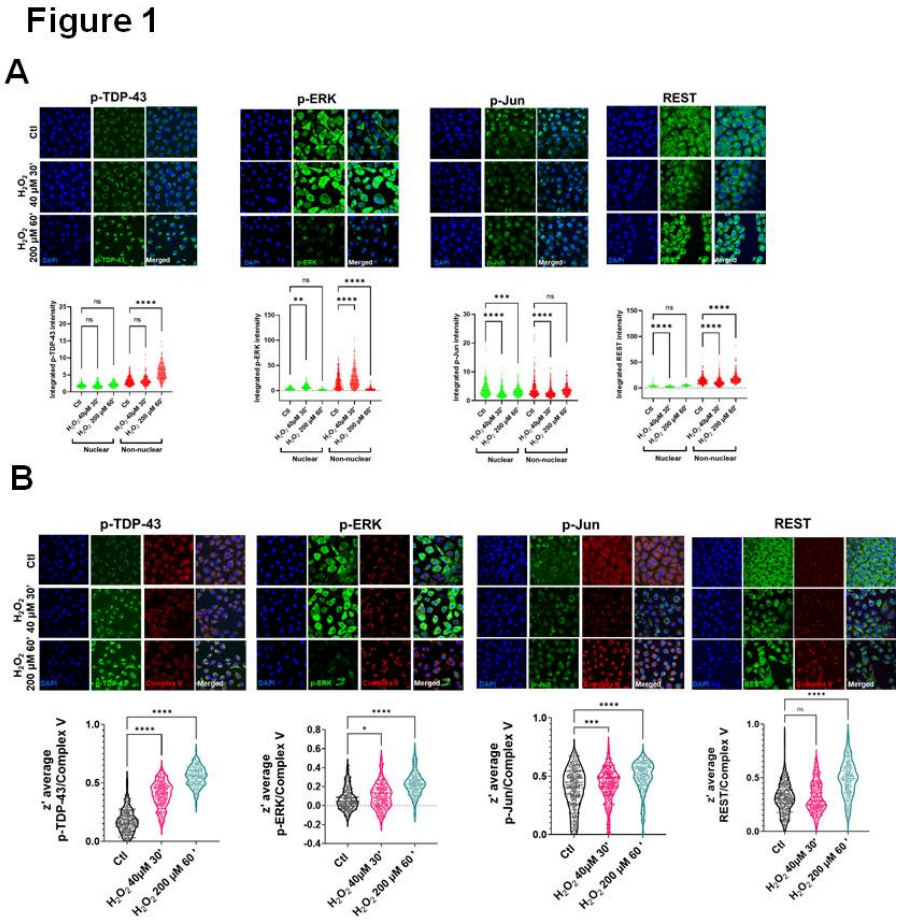

Figure 1. Oxidative stress induces changes in levels of proteins implicated in neurodegeneration and its colocalization with mitochondrial epitopes. A) Representative confocal microscopy images of HMEC cells immunostained with antibodies against p-TDP-43 (left), p-ERK (middle left), p-Jun (middle right) and REST (right) showing diverse effects of oxidative stress (H2O2, dose and time indicated) in nuclear and non-nuclear (cytosol) immunostaining (quantified below).B) Representative coimmunostaining confocal microscopy images of the above mentioned proteins, with mitochondrial epitopes (Complex V). The degree of colocalization was estimated by calculation of the z' factor, shown in the violin graphs below. In A, bars indicate mean with standard deviation shown by lines (n=200 to 296 cells for p-TDP-43; n=191-255 for p-ERK; n=234-326 for p-Jun and n=217-415 for REST, obtained in at least 4 independent replicates). * indicate $p<0.05$, ** $p<0.01$, *** $p<0.001$, and **** $p<0.0001$ by Sidak's post-hoc multiple comparison test after 2 way ANOVA (in A) or by Dunnett's post-hoc multiple comparison test after ANOVA (in B)

Preprints (www.preprints.org) | NOT PEER-REVIEWED | Posted: 9 July 2021 doi:10.20944/preprints202107.0212.v1

These immunostaining results suggested a partial colocalization of mitochondrial epitopes and ALS-related protein factors in a cell line. To validate these results in an independent setup, we evaluated this phenomenon in a murine model of ALS-related neurodegeneration. We employed the TDP-43 Q331K mice, overexpressing the human mutated TDP-43 gene. The results of subcellular fraction in the brain agree with the in vitro findings. Thus, both TDP-43 and ERK are present in crude mitochondria, a subcellular fraction enriched in mitochondria but also containing other membranes (Figure 2A, Supplemental Figure 2). Indeed, as expected, h-TDP-43 was highly enriched in the cytosol, nuclei, and crude mitochondria fraction. Demonstrating that TDP-43 location in crude mitochondria was not an artifact of overexpression of this gene, endogenous (murine) Tdp-43 was also present, as evidenced by western-blot (Figure 2A). Analyses of variance demonstrated that TDP-43 amount was significantly affected by transgenesis (22% of the total variation, $p<0.001$, after three-way ANOVA, Supplemental Table 2). In contrast, subcellular location strongly influenced p-TDP-43 levels (47% of variation, $p<0.0001$), followed by sex (13.6% of the variation, $p<0.0035$), but not transgenesis (Figure 2A, Supplemental Table 2). In general, values of p-TDP-43 were higher in female mice (Figure 2A, Supplemental Figure 2 for males), and in both genders, levels of p-TDP-43 were higher in crude mitochondria than in cytosol (Figure 2A).

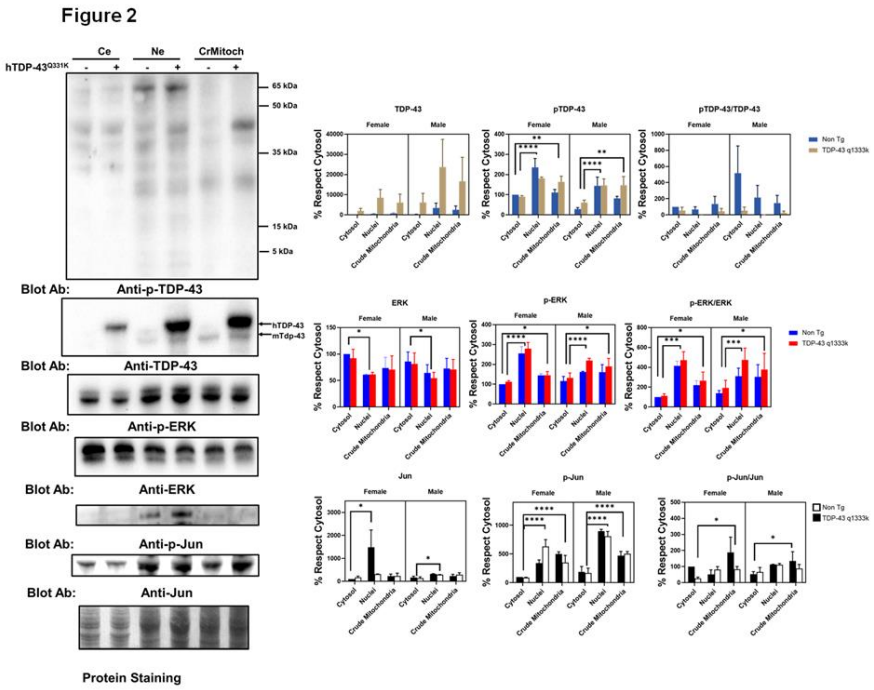

Figure 2. Cellular subfractionation evidence for in vivo colocalization of proteins implicated in neurodegeneration with mitochondrial components. As shown by western-blot analyses of brain lysates after subcellular fractionation, in addition to nuclear enriched (Ne) and cytosolic enriched (Ce) compartments, crude mitochondrial fractions (CrMitoch) both non transgenic and transgenic hTDP-43 mice show the presence of p-TDP-43, p-ERK and Jun. Levels were quantified by densitometry in brains from 90 day old mice. Western-blot shown are for female specimens. Right panels indicate the quantitative analyses. Bars indicate mean values with lines showing standard deviation. * indicate $p<0.05$, ** $p<0.01$, *** $p<0.001$, and **** $p<0.0001$ by Dunnett's post-hoc multiple comparison test after three way ANOVA (n= 4 different mice from each genotype and sex). ANOVA values are shown in text.Concerning ERK, findings in the spinal cord of that murine model reinforce in vitro data. Thus, in line with the colocalization of p-ERK with complex V, crude mitochondria show a relevant concentration of p-ERK. However, nuclear fractions show a high concentration of p-ERK, while total ERK levels were significantly lower in nuclei than cyto-

Preprints (www.preprints.org) | NOT PEER-REVIEWED | Posted: 9 July 2021 doi:10.20944/preprints202107.0212.v1

sol (Figure 2A). Densitometry analyses indicate that total ERK levels were not significantly influenced by sex, transgene expression, or subcellular fraction (Supplemental Table 2). However, when evaluating p-ERK, subcellular location influenced, to the greatest extent, its levels (52% of the variation, $p<0.0001$) with sex interacting with subcellular location also being a relevant factor (13.8%, $p<0.008$).

Regarding p-Jun, we detected its presence mainly in nuclear fractions, with almost no detection in the crude mitochondrial fraction or cytosol. After densitometry, most of the variance was explained by subcellular location (63% of the variance, $p<0.0001$), with sex also influencing the values (9.6%, $p<0.006$). TDP-43 overexpression only explained 4% of the total variance in sex and subcellular location ($p<0.04$, Supplemental Table 2). Nonetheless, we evidenced the presence of Jun in the three fractions examined. Thus, densitometry showed that subcellular location explained more than 16% of the total variance ($p<0.03$, Figure 2, Supplemental Table 1), with no significant influence of sex or TDP-43 overexpression.

Finally, analyses of subcellular fractionation of murine brains revealed that crude mitochondrial fractions, in line with immunostaining measurements, contain a non-negligible amount of REST (Figure 3A). Crude mitochondria were the subcellular fraction with a higher concentration of REST. Regarding the influence of specific factors, neither sex nor TPD-43 overexpression was a significant factor contributing to variance, in contrast to subcellular location (39% of variation, $p<0.0043$, Supplemental Table 2). Besides a nonsignificant trend for an increase in REST in transgenic mice, we evaluated the potential effect of mutated TARDBP overexpression in well-established REST targets by RT-qPCR. The results show that one downstream REST, CYCS mRNA, was increased almost significantly in the TARDBP transgenic mice (Figure 3B).

Preprints (www.preprints.org) | NOT PEER-REVIEWED | Posted: 9 July 2021 doi:10.20944/preprints202107.0212.v1

Figure 3

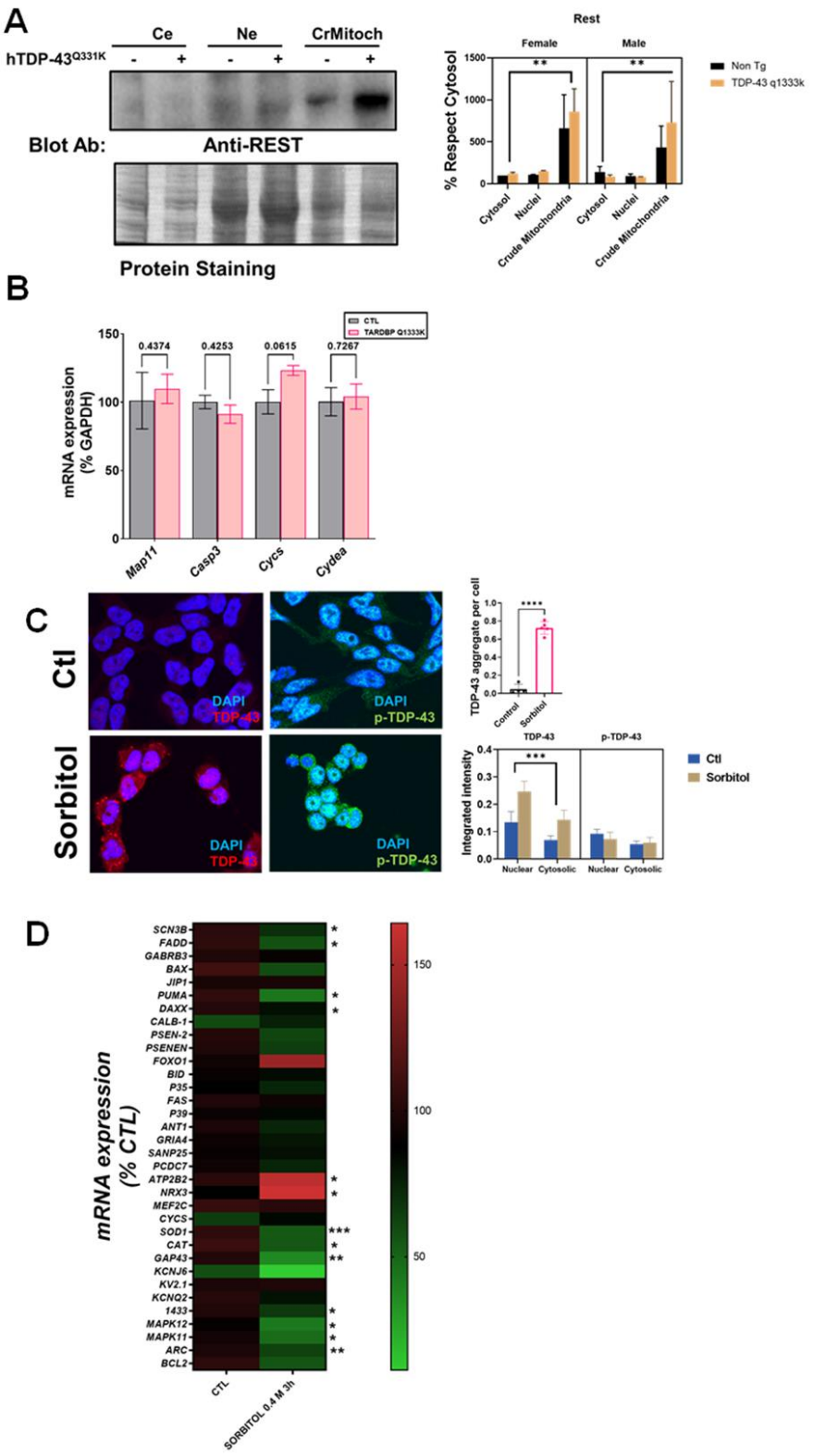

Figure 3. Cell stress-induced mislocalization of TDP-43 is associated to changes in REST regulated genes.A) Shows representative western-blot from brain lysates, indicating that REST is localized within crude mitochondria (CrMitoch), in comparison with enriched nuclei (Ne) or cytosolic extract (Ce). Levels were quantified by densitometry in brains from 90 day old mice (right

Preprints (www.preprints.org) | NOT PEER-REVIEWED | Posted: 9 July 2021 doi:10.20944/preprints202107.0212.v1

panel). Western-blot shown are for female specimens. Bars indicate mean values with lines showing standard deviation. (n=4 different mice from each genotype and sex). B) Shows effect of mutated TARDBP overexpression in the mRNA levels of REST regulated genes in brain lysates, quantified by RT-qPCR. Bars indicate mean values with lines showing standard deviation (n=3 mice from each genotype). C) shows representative immunofluorescence images of N2A cells under osmotic stress (Sorbitol, 0.4 M, 4h), demonstrating that both TDP-43 and p-TDP-43 is localized in a non-nuclear location as aggregates after sorbitol incubation (graphs in right panel). D) shows a heatmap of mRNA expression levels of REST-regulated genes in SHSY-5Y cells under osmotic stress, with the scale in right showing relative overexpression (in red) or downregulation (in green),quantified by RT-qPCR. .* indicate $p<0.05$, ** $p<0.01$, *** $p<0.001$, and **** $p<0.0001$ by Dunnett's post-hoc multiple comparison test after three way ANOVA (in A for integrated intensity of p-TDP-43 or TDP-43 in confocal immunofluorescence analyses or densitometry in C), for Student's t test (in C for the number of aggregates -n=150 different cells quantified in each condition-, or 4 independent RT-qPCR experiments in B or in D).

To further confirm the interaction between TDP-43 and REST, we set up an in vitro model of TDP-43 and p-TDP-43 aggregation in human neural cells (N2A and SHSY-5Y). Thus, after sorbitol incubation (Figure 3C), both the number of TDP-43 aggregates and global intensity of TDP-43, but not p-TDP-43, were increased, with a high amount of TDP-43 in nuclear location. Thus, both subcellular location (18% of the variance, $p<0.0001$) and sorbitol incubation (11.2% of the variance, $p<0.0165$) strongly influenced TDP-43 immunostaining intensity. In this particular model, we explored the effect of REST targets in SHSY-5Y cells. The results of RT-qPCR revealed that TDP-43 aggregation induced by sorbitol incubation was associated with significant decreases in the mRNA levels of SCN3B, FADD, PUMA, DAXX, SOD1, CAT, GAP43, 1433, MAPK11, MAPK12, and ARC, known REST targets. Sorbitol incubation also increased some REST targets such as NRX3 and ATP2B2 (Figure 3D). We also noticed significant increases in CALB-1 and FOXO1 mRNA in mice brain lysates (Figure 3D).

We also examined if other ALS-related cell stressors, such as ER stress, could induce similar delocalizations of the evaluated proteins. We have previously shown that proteasomal and ER stress induces a cytosolic mislocalization of TDP-43[7] . Using similar conditions, we first evaluated if the cells exposed to proteasomal stress (epoxomycin) in similar conditions to the ones already reported to mislocalize TDP-43 also changed p-ERK and p-Jun. The results (Figure 4A) indicate that these proteins exhibited differential dynamics. Thus, in p-ERK, nuclear levels were always inferior to cytosolic ones (90% of total variance explained by cellular location, $p<0001$).

Preprints (www.preprints.org) | NOT PEER-REVIEWED | Posted: 9 July 2021 doi:10.20944/preprints202107.0212.v1

Figure 4

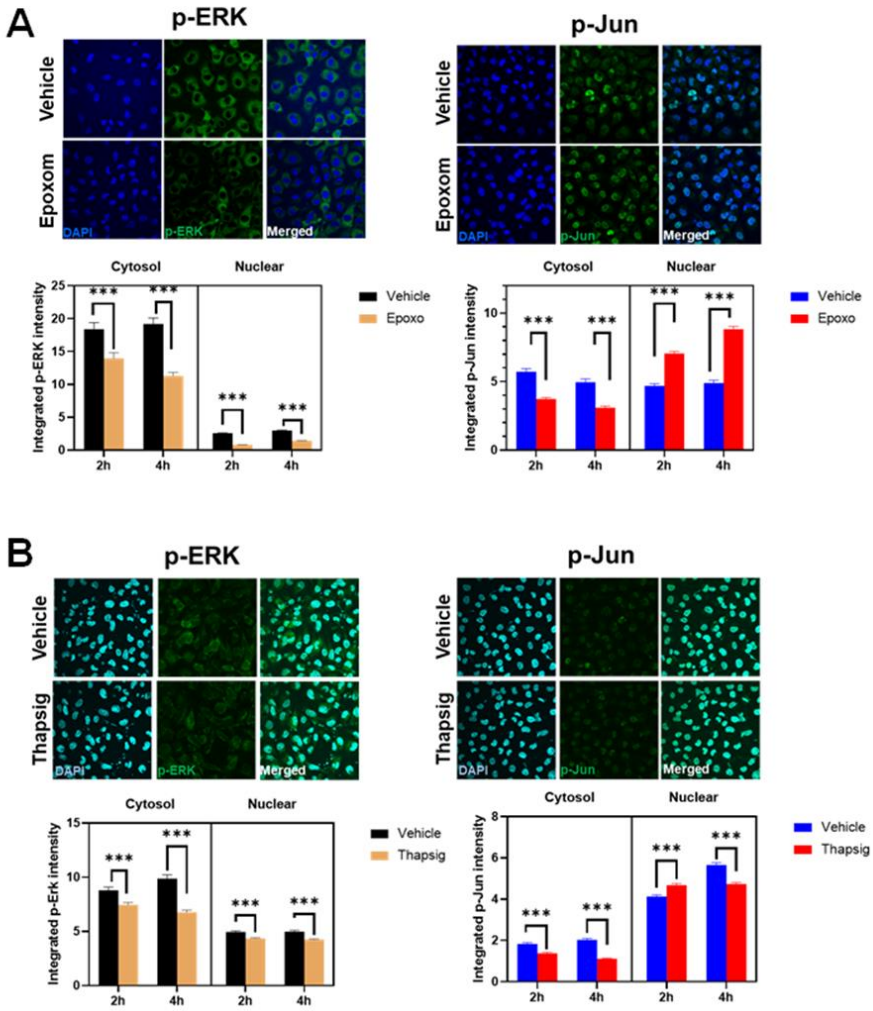

Figure 4. Proteasome and ER stress induces changes in levels p-ERK and p-Jun. Representative confocal microscopy images of HMEC cells immunostained with antibodies against p-ERK and p-Jun showing diverse effects of proteasome inhibition (epoxomicin) in A and ER stress (thapsigargin) in B in nuclear and non-nuclear (cytosol) immunostaining (quantified below). Images shown are for 2 h incubation. In A, bars indicate mean with standard deviation shown by lines (n=195 to 283 cells for p-ERK and n=285-394 for p-Jun); in B (n=519-658 cells for p-ERK and n=415-553 for p-Jun) * indicate $p<0.05$, ** $p<0.01$, *** $p<0.001$, and **** $p<0.0001$ by Sidak's post-hoc multiple comparison test after 2 way ANOVA.

Further, proteasomal stress induced by epoxomycin decreased the levels of p-ERK significantly (either at the nuclei and in the cytosol, 7% of the total variance, $p<0.0001$). In p-Jun, there was a significant interaction between stress and subcellular location, i.e., the effect on epoxomycin depended on the location. Therefore, epoxomycin treatment decreased levels cytosolic levels of p-Jun (Figure 4A), in close relationship with increased levels in the nuclei (51% of total variance explained by the interaction of stress and subcellular location, $p<0.0001$, supplemental Table 3). In the case of ER stress (thapsigargin), we observed similar results in p-ERK. Thus, total levels were decreased after the stress, both at the nuclear and cytosolic levels (Figure 4B). Similarly, the cytosol vs. nuclear location was the factor explaining most variance (79% of total variance,

Preprints (www.preprints.org) | NOT PEER-REVIEWED | Posted: 9 July 2021 doi:10.20944/preprints202107.0212.v1

p<0.0001, supplemental Table 4). For p-Jun, while its preferential nuclear location was maintained, ER stress induced by thapsigargin induced a significant early increase in nuclei (similar to proteasome stress), but later on, levels were decreased, in line with changes in the cytosol (Figure 4B). Therefore, cytosol vs. nuclear location explained most of the variance (90% of variance, p<0.0001, supplemental Table 4).

We then evaluated the potential colocalization of these factors with mitochondrial components. The results of confocal microscopy (Figure 5) suggest that the degree of colocalization was affected by cell stressors. In the case of proteasome stress, the degree of p-ERK colocalization increased significantly at longer times evaluated (Figure 5A), while this was not present for p-Jun. In this later, proteasome stress led to a decrease in the degree of colocalization (Figure 5A). For ER stress, at shorter-term, z'-values increased for p-ERK, but later on, they show a significant decrease (Figure 5B). Both at short and longer times, in the case of p-Jun, decreased degrees of colocalization were evident (Figure 5B).

Figure 5

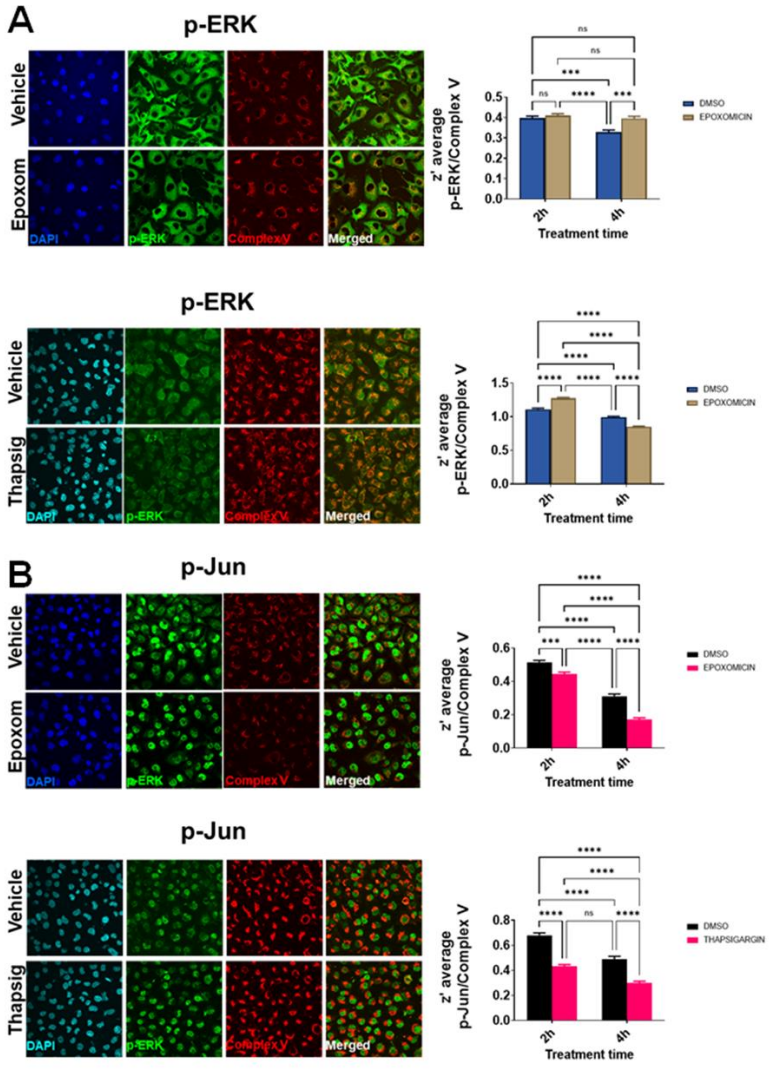

Figure 5. Proteasome and ER stress induces changes in the colocalization degree of p-ERK and p-Jun with mitochondrial epitopes. Representative confocal microscopy images of HMEC cells immunostained with antibodies against p-ERK and mitochondrial epitopes in A and against p-Jun and mitochondrial epitopes in B, showing diverse effects of proteasome inhibition

Preprints (www.preprints.org) | NOT PEER-REVIEWED | Posted: 9 July 2021 doi:10.20944/preprints202107.0212.v1

(epoxomicin) and ER stress (thapsigargin) in the degree of colocalization estimated by calculation of the z' factor (right panels). Bars indicate mean with standard deviation shown by lines (n=195 to 658 cells for p-ERK and n=285-553 for p-Jun); * indicate p<0.05, ** p<0.01, *** p<0.001, and **** p<0.0001 by Bonferroni's post-hoc multiple comparison test after 2 way ANOVA.

To evaluate if the stress mentioned above could be behind the changes in the transgenic TDP-43 model, we also studied the effects of proteasome and ER stress in the levels and distribution of REST in the non-neuronal cell line studied. For epoxomycin treatment, an early (2h) increase in REST intensity in the cytosol was followed by a decrease in the nuclear amount (at 4h, Figure 6A). The degree of colocalization with mitochondrial markers diminished as well (data not shown). Also, the results show that ER stress increased cytosolic and nuclear amount of REST at longer times studied (Figure 6B), also with changes in the degree of colocalization with mitochondria (z values decreased by 20% by epoxomycin treatment, data not shown).

Figure 6

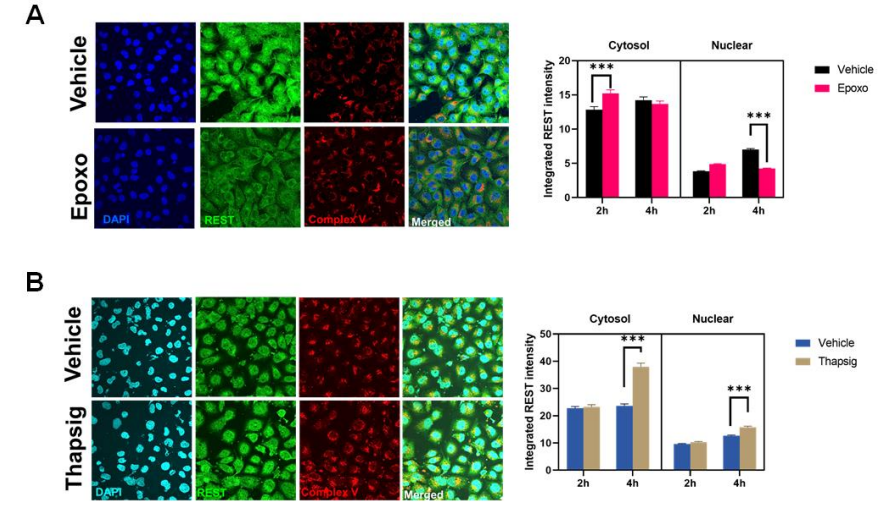

Figure 6. ER and proteasome stress induces changes in levels of REST and its colocalization with mitochondrial epitopes. Representative confocal microscopy images of HMEC cells immunostained with antibodies against REST and mitochondrial complex V showing diverse effects of proteasome stress (A) and ER stress (B) (n=365-559 different cells). In right graphs bars indicate mean with standard deviation shown by lines *** indicate p<0.001 by Sidak's post-hoc multiple comparison test after 2 way ANOVA.

Preprints (www.preprints.org) | NOT PEER-REVIEWED | Posted: 9 July 2021 doi:10.20944/preprints202107.0212.v1

3. Discussion

This work shows that several proteins implicated in ALS (TDP-43, ERK) and other neurodegenerative processes, such as AD(Jun, REST), show sensitivity to cell stress. Several neurodegenerative diseases exhibit protein aggregates where these proteins may be present[19]. We evaluated three different major cellular stressors, namely oxidative stress, proteasome inhibition, and ER stress, and we demonstrate that the effects on cellular distribution show stress and protein specificity.

In the case of TDP-43, the results show that after oxidative stress or osmotic stress, cytosolic levels of this protein increase both in the endothelial cell line and in neuronal cell lines. Further, the degree of colocalization within mitochondria also increased. Of note, TDP-43 may show differences of behavior with p-TDP-43. Thus, while TPD-43 is accumulated after sorbitol stress in the cytosol, nonsignificant were present with P-TDP-43. The in vivo evidence presented shows that this is also the case in the brain lysates, where p-TDP-43 and TDP-43 show differential responses to overexpression of mutated TARDBP. Whatever the case, subcellular fractionation data agree with enrichment of both endogenous murine tdp-43 and hTDP-43 in mitochondrially enriched fractions.

Regarding ERK, in response to increased oxidative stress, we noticed a decrease in the cytosolic and nuclear locations after a transient increase. Nonetheless, the degree of colocalization increased significantly, suggesting the close occurrence of p-ERK with mitochondrial epitopes again. In contrast with p-TDP-43, slopes relating to nuclear and extranuclear p-ERK were inversely related to oxidative stress intensity, suggesting nuclear retention of this factor or rapid cytosolic clearance of it. The same phenomena (decrease both in the cytosol and in nuclei) was present after proteasome and ER stress. This later cell stress also decreased the colocalization within mitochondrial epitopes. Interestingly, after epoxomicin treatment, we observed an increase in the degree of mitochondrial colocalization. Subcellular fractionation in the TDP-43 model suggested that p-ERK could be significantly enriched with mitochondria, independently of TARDBP overexpression.

Concerning p-Jun, no clear accumulation in extranuclear location was present after oxidative stress, though mitochondrial colocalization increased. After proteasome inhibition and ER stress, extranuclear levels of this factor were decreased with concomitant retention in nuclei (thought at later stages, ER stress decreased levels of nuclear p-Jun slightly). In clear contrast with oxidative stress, both ER stress and proteasome inhibition decreased mitochondrial colocalization. Indeed, subcellular fractionation suggested that while Jun accumulated with crude mitochondria, this was not the case with p-Jun.

Regarding REST, its accumulation has been previously reported in a cytosolic location in neurodegenerative processes. Our data regarding response to cell stress show that its behavior was similar to p-Jun, showing an initial decrease in cytosol followed by a slight increase in both nuclei and cytosol. Epoxomycin treatment decreased nuclear levels after the long exposure, while ER stress increased their values in the cytosol and nuclei. Indeed, the degree of colocalization increased after oxidative stress. Previous data also reported the relationship between changes in REST expression and protein aggregates[20]. Particularly, several genes under the control of this negative regulator are upregulated, suggesting its impairment in human pathology[20]. Amongst the controlled genes, the authors indicated increased ubiquitin carboxy-terminal hydrolase L1, a component of the aggregates[20]. This protein is involved in the ubiquitin-proteasome pathway of proteostasis, suggesting that REST could influence proteostasis. Our data indicate that the reverse is also true, i.e. proteasome could control REST protein levels and their subcellular location.

Preprints (www.preprints.org) | NOT PEER-REVIEWED | Posted: 9 July 2021 doi:10.20944/preprints202107.0212.v1

Interestingly, in vivo data show that overexpression of mutated TARDBP increased the degree of REST enrichment in mitochondrial fractions. The interaction between TDP-43 alterations and REST is new, and it is reinforced by the fact that several REST-regulated genes appear affected under osmotic stress conditions, where TDP-43 is mislocalized. These genes included SCN3B, encoding a voltage-gated sodium channel[21], and two genes implicated in apoptosis (PUMA and FADD)[22], with downregulation in both cases. Interestingly, in human cells evaluated, sorbitol decreased the expression of transcripts encoding antioxidant enzymes, such as SOD1 and catalase. Furthermore, in these cells, an increased expression of the ATP2B2 mRNA was found, encoding a plasma membrane Ca++ pump. Also, we noticed decreased ARC mRNA expression in cells, implicating altered mRNA traffic (one of the functions of TDP-43). We also detected decreased p35 mRNA after osmotic stress. P35 is a neuron-specific cyclin-dependent kinase 5 activator. The activation of this factor is necessary for appropriate central nervous system development[23]. Calpain proteolytically cleaves the p35 form of this protein, resulting in the p25 form. When p35 is cleaved into p25, the protein is relocalized from the cell periphery to the nucleus, and perinuclear region. Patients with AD accumulate the p25 form in their brain neurons[24]. This buildup is linked to an increase in CDK5 kinase activity, leading to abnormally phosphorylated microtubule forms. CDK5 kinase overactivation is linked to TDP-43 pathological effects in neuronal cells[25]. We also detected increased Foxo 1 mRNA. It is known that this key metabolic transcription factor promotes neuron death [26]. Therefore decreased values of antiapoptotic factors (PUMA and FADD) may be responses to this increased expression.

Accounting for the fact that one of their primary functions is working as transcription factors (in the case of ERK, Jun, and REST) or interacting with RNA (in the case of TDP-43), their localization in extranuclear placements (particularly in close relationships with mitochondrial epitopes) suggest the existence of pathogenic mechanisms operating in common. All these factors require nucleocytosolic transport; therefore, a loss in this cellular property's homeostasis may partially explain their presence in the cytosol. Indeed, we have recently reported that nuclear envelope (where the proteins responsible for nucleocytoplasmic shuttling reside) show altered properties in ALS patients and models.

Several reports have described the occurrence of TDP-43 in mitochondrial fractions[27] and other membranal fractions[18]. Regarding Jun, it is known that its N-terminal kinase (JNK) is located in mitochondria[28]. Other studies demonstrate that cytosolic location of c-Jun depends of its interaction with other transcription factors[29]. Of note, the major location of p-Jun in brain lysates is nuclei, but we detect a consistent signal in cytosol and in crude mitochondrial fractions. Previous in vitro studies show that c-Jun interacts with phospholipids[30].Interestingly, other in vivo reports indicate that cytoplasmic c-Jun is associated with mitochondria[31]. Indeed, it is known that c-Jun may interact with mitochondrial DNA motifs, being mitochondrial location validated by electron microscopy [32]. Despite some doubts for the mitochondrial location of typically nuclear transcription factors, such as NF-kB[33], it may be adequate to validate the reported findings further and establish the interaction of c-Jun with mitochondria. Further c-Jun binding sites occur within mtDNA genes and are negatively selected[32]. It has been suggested that oxidative phosphorylation, mitochondrial translation, and mtDNA repair processes.

Regarding p-ERK, it is known that there are mitochondrial substrates for its kinase activity[34]. Recent data underlines that ERK signaling specificity requires spatial compartmentalization of ERK activity for signals like EGF to govern diverse functional responses via compartmentalized ERK activity[35]. Previous data showed that p-ERK mitochondrial location could be a consequence of tumoral transformation[36] demonstrating that a fraction of active ERK1/2 associates with succinate dehydrogenase and some mitochondrial chaperones, such as TRAP1[37].We have previously shown that motor neurons in spinal cord from ALS patients exhibit p-ERK aggregates in extranuclear locations[7].

Preprints (www.preprints.org) | NOT PEER-REVIEWED | Posted: 9 July 2021 doi:10.20944/preprints202107.0212.v1

These aggregates may be related potentially to mitochondrial interaction. In this regard, we show that there are no interactions between p-ERK and TDP-43 overexpression in the evaluated murine model.

To the best of our knowledge, we have not found previous evidence of REST in mitochondria. Previous evidence in human substantia nigra [10] show a cytoplasmic staining profile in neurons. Nonetheless, in this publication, REST is found as aggregates, closely related to autophagy impairment[38]. Thus, defects in the protein quality control system induce REST mRNA expression; its gene product mainly appears in aggregates. In brain subcellular fractionation experiments, we did not evidence changes in total levels of REST. Nonetheless, we show that all stress evaluated, including ER, proteasomal, and oxidative stress changes its cellular distribution, increasing the colocalization with mitochondrial epitopes. Indeed, recent data show that CRISPR-mediated REST KO induced mitochondrial dysfunction and impaired mitophagy in vitro. Furthermore, REST overexpression impedes mitochondrial toxicity and mitochondrial morphology disruption through the transcription factor PGC-1α [39].

As for the limitations of our work, we must remark that this evidence was present in an endothelial-like cell phenotype. Therefore, neuronal or glial cells could exhibit different dynamics. Nonetheless, some of the findings in the endothelial cell culture were replicated independently in lysates of the brain cortex of a murine model, and in N2a and SHSY-5y cells, human neuronal lines further validate the potential findings. We shall also indicate that the subcellular fractionation was more enriching than a strict purification of the indicated compartment. However, we can exclude nuclear contamination of mitochondrial fraction (based on purity markers).In conclusion, cell stress enhances the non-nuclear localization of transcription factors, increasing its interaction with mitochondria and potentially cross influencing their physiology (as shown for the TDP-43-REST interaction).

4. Materials and Methods

4.1 Animals

According to local laws and the Directive 2010/63/EU of the European Parliament, all experimental procedures were approved by the Institutional Animal Care Committee of the University of Lleida. The minimal number of animals was calculated according to the deviation of western-blot profiles in previous experiments [18].Both non transgenic and transgenic mice were obtained from JAX. Transgenic mice were from the line B6.Cg-Tg(Prnp-TARDBP*Q331K)103Dwc/J (Stock number #017933). These mice express, employing the murine prion-promoter previously reported to drive transgene expression most abundantly in the central nervous system, both in neurons and astrocytes, ALS-linked mutant TDP-43 broadly throughout the central nervous system [40]. Under the control of the murine prion promoter, transgenic mice expressed the ALS-linked mutant of TDP-43 [41][Q331K (glutamine to lysine substitution at amino acid position 331) fused to an N-terminal myc-tag. Animals employed here were from both sexes (at least n=5 different mice from each sex) and from 90 days old, an age where the motor phenotype is not present. Housing and obtention of animals were as described[40,42]. For animal sacrifice, mice were anesthetized with 2.5% isoflurane.Brains were rapidly excised and maintained at 4ºC in isolation buffer for a maximum time of 15 min, being submitted to subcellular fractionation.

4.2 Subcellular fractionation

Purification of nuclear, mitochondria and cytosol enriched fractions performed as described[43]. Briefly, brain samples were homogenized gently in isolation buffer (225 mmol/L mannitol, 25 mmol/L HEPES-KOH, and 1 mmol/L EGTA, pH 7,4 containing pro-

Preprints (www.preprints.org) | NOT PEER-REVIEWED | Posted: 9 July 2021 doi:10.20944/preprints202107.0212.v1

tease inhibitors (78429 Thermo Scientific) and Sodium Fluoride and Sodium Orthovanadate as phosphatase inhibitors) with 10-12 strokes in a glass tissue grinder. The homogenate was centrifuged for 10 minutes at 1500 × g to obtain a nuclei enriched fraction. The supernatant was washed twice by centrifuging for 10 minutes at 1,500 × g to eliminate any residual whole cells and cell debris. Supernatant obtained was centrifuged for 15 minutes at 10,000 × g; the supernatant contained the ER/cytosol fraction and the pellet contained the crude mitochondrial fraction. The ER/cytosol fraction was centrifuged for 1 hour at 100,000 × g in a ultracentrifuge and the supernatant was considered cytosol.

4.3 Cell culture

Human mammary epithelial cells (HMEC) cell line (ATCC# PCS-600-010™) was grown in DMEM medium (Invitrogen) supplemented with 10% fetal bovine serum heat inactivated (Invitrogen), 2 mM L-Glutamine (Invitrogen) and 20 U/ml penicillin and 20 µg/ml streptomycin (Invitrogen) as antibiotics. The cells were kept at 37 ºC in humidify atmosphere with 5% of CO2.

N2A and SHSY-5Y (ATCC) cell lines were grown in Advanced MEM medium (Invitrogen) supplemented with 10% fetal bovine serum heat inactivated (Invitrogen), 2 mM L-Glutamine (Invitrogen) and 20 U/ml penicillin and 20 µg/ml streptomycin (Invitrogen) as antibiotics. The cells were kept at 37 ºC in humidify atmosphere with 5% of CO2.

To study the effects of oxidative stress, alteration of endoplasmic reticulum, inhibition of proteasome activity and osmotic stress, cells were treated with 10 µM H2O2 (Sigma), 5 µM thapsigargin (Thp) (Sigma), 2.5 µM epoxomicin (Epox) (Sigma) respectively, for 2 or 4 h or sorbitol (Sigma) 0.4 M for 3 h. To avoid the influence of growth factors present in the fetal bovine serum on the results, the normal culture medium was replaced by Optimem before 12h before all assays (Invitrogen, Carlsbad, CA, USA), as described[7].

4.4 Indirect immunofluorescence analysis

Cells, seeded out on coverslips and incubated in serum and phenol red free medium (Optimem, Invitrogen) for 12 hours, were treated as indicated above. After incubation, cells were washed with PBS and then fixed with 3.7% paraformaldehyde for 10 min at room temperature. Cells were rinsed with PBS, permeabilized with 0.1% Triton X-100 in PBS for 30 min and subsequently blocked with 5% normal goat serum at room temperature for 1 hour. Cells were incubated with (1) the mouse anti-p-TDP-43 (pS409/410) monoclonal antibody (TIP-PTD-M01) (diluted 1:200, Cosmo Bio Co.); (3) the rabbit anti-p-ERK 1/2 polyclonal antibody (4370) (diluted 1:100, Cell Signaling, Beverly, MA, USA); the rabbit anti-REST polyclonal antibody (ab21635) (diluted 1:100, Abcam,Cambridge, UK); (4) the rabbit anti p-Jun polyclonal antibody (diluted 1:100, Cell Signaling, Beverly, MA, USA); (5) the anti-ATP5A mouse monoclonal antibody (ab14748) (diluted 1:100, Abcam, Cambridge, UK) at 4ºC overnight. After 3 washes with 0.1% Triton X-100-PBS at RT for 10 min, cells were incubated with Alexa Fluor-488 goat anti-rabbit IgG or Alexa-Fluor-594 goat anti-mouse IgG (1:800, Molecular Probes) conjugated secondary antibody. Nuclei were stained with 4′,6′-diamino-2-phenylindole (DAPI) (1mg/ml, Sigma). The coverslips were mounted in Fluoromount-G (Southern Biotech) and images were taken with a Olympus FV10i laser scanning confocal microscope and a Olympus FV1000 confocal microscopy, 60X magnification. For the evaluation of nuclear and cytosolic protein intensity we used a dedicated pipeline created on the open source CellProfiler software[44]. Another CellProfiler pipeline was built to evaluate colocalization with the mitochondrial marker ATP5A. In both cases, 10 fields per condition were analyzed. CellProfiler pipelines employed are available in supplemental data.

4.5 Western-blot

Preprints (www.preprints.org) | NOT PEER-REVIEWED | Posted: 9 July 2021 doi:10.20944/preprints202107.0212.v1

Protein homogenates were prepared in the presence of inhibitors of phosphatases (Sigma-Aldrich) and proteases (Roche Applied Science, Penzberg, Germany). Protein concentration of the samples was measured using the Quick Start™ Bradford 1x Dye Reagent(Bio-Rad #5000205). Proteins were detected by immunoblotting using horseradish peroxidase-conjugated secondary antibodies and chemiluminescence (Santa Cruz Biotechnology). Protein samples were ran on SurePAGETM Precast gels (4-20%, 15 wells GenScript, Piscataway, NJ) . Gels were blotted onto PVDF membranes by transfer at a constant 100 volts, 1 hour at RT. The membranes were then blocked by non-fat dry milk solution (5%) in 1 × TBS (Tris Buffered Saline) and incubated in the desired primary antibody overnight.

Membranes were then washed in 1 × TBST with Tween 20 (0.05%) three times, 5 min each before incubating with the secondary antibody for 1 h at room temperature. Following the secondary antibody incubation, membranes were washed in 1 x TBST with Tween 20 (0.05%) three times, 5 min each and one time, 5 min, with TBS 1 x. Blots were imaged in the Chemidoc MP Imaging System following incubation in the Immobilon ECL Ultra Western HRP Substrate (Merck Millipore, Burlington, USA).

For Jun/ p-c-Jun westerns, protein samples were ran on SurePAGETM Precast gels (4-20%, 15 wells GenScript, Piscataway, NJ). Cruz Marker™ molecular weight standards (sc-2035) were loaded in the gels. Gels were blotted onto low fluorescence PVDF membranes (Immobilon®-FL PVDF: sc-516541). Non-specific binding was blocked yb incubating membranes with UltraCruz® Blocking Reagent (sc-516214) for 1 hour at room temperature, with shaking.

The blocked membranes were incubated with the appropriates Alexa Fluor® conjugated primary antibodies (Anti-p-c-Jun Antibody (KM-1) Alexa Fluor® 790 and Anti c-Jun Antibody (G-4) Alexa Fluor® 680) diluted 1:1000 in UltraCruz® Blocking Reagent. Cruz Marker™ MW Tag-Alexa Fluor® 680 (sc-516730) and Cruz Marker™ MW Tag-Alexa Fluor® 790 (sc-516731) at 1:1000 were added.

Membranes were incubated in this mixture for 2 hours at room temperature, in the dark, with shaking. Membranes were then washed three times for 5 minutes each with TBST and once for 5 minutes with TBS. Blots when then placed on the top of blotter paper and dried for 5-10 minutes. The western blot was imaged using the infrared (IR) laser-based instrumentation LI-COR Odyssey (Lincoln, NE, USA).

4.6 RT-QPCR

RNA was extracted from cells and brain lysates using TRI Reagent (Thermo Fisher Scientific, AM9738) following the manufacturer's instructions. RNA concentrations were measured using a NanoDrop ND-1000 (Thermo Fisher Scientific). One microgram of RNA was used for retrotranscription to cDNA employing TaqMan Reverse Transcription Reagent and random hexamers (Thermo Fisher Scientific, N8080234).

RT-qPCR experiments were performed using a CFX96 instrument (Bio-Rad, Hercules, California, USA) with SYBR Select Master mix for CFX (Thermo Fisher Scientific, 4472937). Each 20 µL reaction mix contained 4µL cDNA, 10 µL SYBR Select Master Mix, 0.2 nM of forward primer and 0.2 nM of reverse primer solutions and 4 µL PCR grade water. RT-qPCR run protocol was as follows: 50 °C for 2 minutes and 95 °C for 2 minutes, with the 95 °C for 15 seconds and 60 °C for 1 minute steps repeated for 40 cycles; and a melting curve test from 65°C to 95 °C at a 0.1 °C/s measuring rate. Primers employed in these experiments, previously described in[9] are listed in Supplemental Table 5.

4.7 Statistical analysis

All statistics were performed using the GraphPad Prism version9.1.2 for Windows software (GraphPad Software, San Diego, California USA, www.graphpad.com) Differences between groups were analyzed by the Student's t tests, One way, Two way and

Preprints (www.preprints.org) | NOT PEER-REVIEWED | Posted: 9 July 2021 doi:10.20944/preprints202107.0212.v1

Three-way ANOVA analyses, with adequate post-hoc analyses, once normality of variables was tested by Kolmogorov-Smirnov test. The 0.05 level was selected as the point of minimal statistical significance in every comparison.

Supplementary Materials: The following are available online at www.mdpi.com/xxx/s1, Figure S1: Oxidative stress induces changes between the nucleocytosolic relationships of proteins implicated in neurodegeneration, Figure S2: Enrichment of protein markers in subcellullar fractionation,Figure S3 Cellular subfractionation evidence for in vivo colocalization of proteins implicated in neurodegeneration with mitochondrial components in male mice; :, Supplemental Table 1. Effect of H2O2 treatment in protein subcellular distribution by confocal microscopy; Supplemental Table 2. Effect of mutated TARDBP overexpression in subcellular distribution of transcription factors; Supplemental Table 3: Effect of Epoxomycin treatment in protein subcellular distribution by confocal microscopy; Supplemental Table 4. Effect of thapsigargin treatment in protein subcellular distribution by confocal microscopy, Supplemental Table 5. Primers employed for quantitation of REST transcriptional regulation. Pipelines for Cellprofiler quantitative analyses are also available in the web.

Author Contributions: Conceptualization, M.P-O., I.F. and R.P.; methodology, C.R., A.G-S and O.R-N.; software, C.R.; validation, M.P.; formal analysis, C.R., P.T..; investigation, C.R..; resources, P.T., C.R., A.F.; data curation, R.P.; writing—original draft preparation, C.R.; writing—review and editing, M P.O

Funding: This research was funded by the Spanish Ministry of Economy and Competitiveness, Institute of Health Carlos III (PI 17–00134,PI20-0155) to M.P-O; from the Spanish Ministry of Science, Innovation, and Universities (RTI2018-099200-B-I00), and the Generalitat of Catalonia (Agency for Management of University and Research Grants (2017SGR696) and Department of Health (SLT002/16/00250) to RP. PT was a predoctoral fellow from the Ministerio de Educacion (FPU16/01446). CR held predoctoral fellowship "Ajuts 2020 de Promoció de la Recerca en Salut-8ª edició" from IRBLleida/Diputació de Lleida. Support was also received in the form of a Fundación Española para el Fomento de la Investigación de la Esclerosis Lateral Amiotrófica (FUNDELA] Grant, RedELA-Plataforma Investigación, and the Fundació Miquel Valls (Jack Van den Hoek donation]. This study has been co-financed by FEDER funds from the European Union ("A way to build Europe"). IRBLleida is funded by a Centres de Recerca de Catalunya (CERCA) Programme/Generalitat of Catalonia.

Institutional Review Board Statement: The study was conducted according to the guidelines of the Declaration of Helsinki, and approved by the Institutional Review Board of Universitat de Lleida (protocol CEEA 18-01/12, 2012-06-01)

Informed Consent Statement: Not applicable
Data Availability Statement: Raw data are available from the authors on reasonable request.

Conflicts of Interest: The authors declare no conflict of interest.

References

1. Ross, C. A.; Poirier, M. A. Protein aggregation and neurodegenerative disease. Nat. Med. 2004, 10 Suppl, S10–7, doi:10.1038/nm1066.
2. Colombrita, C.; Zennaro, E.; Fallini, C.; Weber, M.; Sommacal, A.; Buratti, E.; Silani, V.; Ratti, A. TDP-43 is recruited to stress granules in conditions of oxidative insult. J. Neurochem. 2009, 111, 1051–1061, doi:10.1111/j.1471-4159.2009.06383.x.
3. Prasad, A.; Bharathi, V.; Sivalingam, V.; Girdhar, A.; Patel, B. K. Molecular Mechanisms of TDP-43 Misfolding and Pathology in Amyotrophic Lateral Sclerosis. Front. Mol. Neurosci. 2019, 12, 25, doi:10.3389/fnmol.2019.00025.
4. McDonald, K. K.; Aulas, A.; Destroismaisons, L.; Pickles, S.; Beleac, E.; Camu, W.; Rouleau, G. A.; Vande Velde, C. TAR DNA-binding protein 43 (TDP-43) regulates stress granule dynamics via differential regulation of G3BP and TIA-1. Hum. Mol. Genet. 2011, 20, 1400–1410, doi:10.1093/hmg/ddr021.
5. Guerrero, E. N.; Wang, H.; Mitra, J.; Hegde, P. M.; Stowell, S. E.; Liachko, N. F.; Kraemer, B. C.; Garruto, R. M.; Rao, K. S.; Hegde, M. L. TDP-43/FUS in motor neuron disease: Complexity and challenges. Prog. Neurobiol. 2016, 145-146, 78–97, doi:10.1016/j.pneurobio.2016.09.004.
6. Woerner, A. C.; Frottin, F.; Hornburg, D.; Feng, L. R.; Meissner, F.; Patra, M.; Tatzelt, J.; Mann, M.; Winklhofer, K. F.; Hartl, F. U.; Hipp, M. S. Cytoplasmic protein aggregates interfere with nucleocytoplasmic transport of protein and RNA. Science 2016, 351, 173–176, doi:10.1126/science.aad2033.
7. Ayala, V.; Granado-Serrano, A. B.; Cacabelos, D.; Naudí, A.; Ilieva, E. V.; Boada, J.; Caraballo-Miralles, V.; Lladó, J.; Ferrer, I.; Pamplona, R.; Portero-Otin, M. Cell stress induces TDP-43 pathological changes associated with ERK1/2 dysfunction: implications in ALS. Acta Neuropathol. 2011, 122, 259–270, doi:10.1007/s00401-011-0850-y.

Preprints (www.preprints.org) | NOT PEER-REVIEWED | Posted: 9 July 2021 doi:10.20944/preprints202107.0212.v1

8. Meyerowitz, J.; Parker, S. J.; Vella, L. J.; Ng, D. C.; Price, K. A.; Liddell, J. R.; Caragounis, A.; Li, Q.-X.; Masters, C. L.; Nonaka, T.; Hasegawa, M.; Bogoyevitch, M. A.; Kanninen, K. M.; Crouch, P. J.; White, A. R. C-Jun N-terminal kinase controls TDP-43 accumulation in stress granules induced by oxidative stress. Mol. Neurodegener. 2011, 6, 57, doi:10.1186/1750-1326-6-57.
9. Lu, T.; Aron, L.; Zullo, J.; Pan, Y.; Kim, H.; Chen, Y.; Yang, T.-H.; Kim, H.-M.; Drake, D.; Liu, X. S.; Bennett, D. A.; Colaiácovo, M. P.; Yankner, B. A. REST and stress resistance in ageing and Alzheimer's disease. Nature 2014, 507, 448–454, doi:10.1038/nature13163.
10. Kawamura, M.; Sato, S.; Matsumoto, G.; Fukuda, T.; Shiba-Fukushima, K.; Noda, S.; Takanashi, M.; Mori, N.; Hattori, N. Loss of nuclear REST/NRSF in aged-dopaminergic neurons in Parkinson's disease patients. Neurosci. Lett. 2019, 699, 59–63, doi:10.1016/j.neulet.2019.01.042.
11. Chou, C.-C.; Zhang, Y.; Umoh, M. E.; Vaughan, S. W.; Lorenzini, I.; Liu, F.; Sayegh, M.; Donlin-Asp, P. G.; Chen, Y. H.; Duong, D. M.; Seyfried, N. T.; Powers, M. A.; Kukar, T.; Hales, C. M.; Gearing, M.; Cairns, N. J.; Boylan, K. B.; Dickson, D. W.; Rademakers, R.; Zhang, Y.-J.; Petrucelli, L.; Sattler, R.; Zarnescu, D. C.; Glass, J. D.; Rossoll, W. TDP-43 pathology disrupts nuclear pore complexes and nucleocytoplasmic transport in ALS/FTD. Nat. Neurosci. 2018, 21, 228–239, doi:10.1038/s41593-017-0047-3.
12. Cook, C. N.; Wu, Y.; Odeh, H. M.; Gendron, T. F.; Jansen-West, K.; Del Rosso, G.; Yue, M.; Jiang, P.; Gomes, E.; Tong, J.; Daughrity, L. M.; Avendano, N. M.; Castanedes-Casey, M.; Shao, W.; Oskarsson, B.; Tomassy, G. S.; McCampbell, A.; Rigo, F.; Dickson, D. W.; Shorter, J.; Zhang, Y.-J.; Petrucelli, L. C9orf72 poly(GR) aggregation induces TDP-43 proteinopathy. Sci. Transl. Med. 2020, 12, doi:10.1126/scitranslmed.abb3774.
13. Nishimura, A. L.; Zupunski, V.; Troakes, C.; Kathe, C.; Fratta, P.; Howell, M.; Gallo, J.-M.; Hortobágyi, T.; Shaw, C. E.; Rogelj, B. Nuclear import impairment causes cytoplasmic trans-activation response DNA-binding protein accumulation and is associated with frontotemporal lobar degeneration. Brain 2010, 133, 1763–1771, doi:10.1093/brain/awq111.
14. Ramírez-Nuñez, O.; Jové, M.; Torres, P.; Sol, J.; Fontdevila, L.; Romero-Guevara, R.; Andrés-Benito, P.; Ayala, V.; Rossi, C.; Boada, J.; Povedano, M.; Ferrer, I.; Pamplona, R.; Portero-Otin, M. Nuclear lipidome is altered in amyotrophic lateral sclerosis: A pilot study. J. Neurochem. 2021, doi:10.1111/jnc.15373.
15. Wang, W.; Wang, L.; Lu, J.; Siedlak, S. L.; Fujioka, H.; Liang, J.; Jiang, S.; Ma, X.; Jiang, Z.; da Rocha, E. L.; Sheng, M.; Choi, H.; Lerou, P. H.; Li, H.; Wang, X. The inhibition of TDP-43 mitochondrial localization blocks its neuronal toxicity. Nat. Med. 2016, 22, 869–878, doi:10.1038/nm.4130.
16. Wang, P.; Deng, J.; Dong, J.; Liu, J.; Bigio, E. H.; Mesulam, M.; Wang, T.; Sun, L.; Wang, L.; Lee, A. Y.-L.; McGee, W. A.; Chen, X.; Fushimi, K.; Zhu, L.; Wu, J. Y. TDP-43 induces mitochondrial damage and activates the mitochondrial unfolded protein response. PLoS Genet. 2019, 15, e1007947, doi:10.1371/journal.pgen.1007947.
17. Joshi, V.; Upadhyay, A.; Prajapati, V. K.; Mishra, A. How autophagy can restore proteostasis defects in multiple diseases? Med Res Rev 2020, 40, 1385–1439, doi:10.1002/med.21662.
18. Gautam, M.; Jara, J. H.; Kocak, N.; Rylaarsdam, L. E.; Kim, K. D.; Bigio, E. H.; Hande Özdinler, P. Mitochondria, ER, and nuclear membrane defects reveal early mechanisms for upper motor neuron vulnerability with respect to TDP-43 pathology. Acta Neuropathol. 2019, 137, 47–69, doi:10.1007/s00401-018-1934-8.
19. Spires-Jones, T. L.; Attems, J.; Thal, D. R. Interactions of pathological proteins in neurodegenerative diseases. Acta Neuropathol. 2017, 134, 187–205, doi:10.1007/s00401-017-1709-7.
20. Barrachina, M.; Moreno, J.; Juvés, S.; Moreno, D.; Olivé, M.; Ferrer, I. Target genes of neuron-restrictive silencer factor are abnormally up-regulated in human myotilinopathy. Am. J. Pathol. 2007, 171, 1312–1323, doi:10.2353/ajpath.2007.070520.
21. O'Malley, H. A.; Isom, L. L. Sodium channel β subunits: emerging targets in channelopathies. Annu. Rev. Physiol. 2015, 77, 481–504, doi:10.1146/annurev-physiol-021014-071846.
22. Ola, M. S.; Nawaz, M.; Ahsan, H. Role of Bcl-2 family proteins and caspases in the regulation of apoptosis. Mol. Cell. Biochem. 2011, 351, 41–58, doi:10.1007/s11010-010-0709-x.
23. Dhariwala, F. A.; Rajadhyaksha, M. S. An unusual member of the Cdk family: Cdk5. Cellular and molecular neurobiology 2008.
24. Patrick, G. N.; Zukerberg, L.; Nikolic, M.; de la Monte, S.; Dikkes, P.; Tsai, L. H. Conversion of p35 to p25 deregulates Cdk5 activity and promotes neurodegeneration. Nature 1999, 402, 615–622, doi:10.1038/45159.
25. Rao, M. V.; Campbell, J.; Palaniappan, A.; Kumar, A.; Nixon, R. A. Calpastatin inhibits motor neuron death and increases survival of hSOD1(G93A) mice. J. Neurochem. 2016, 137, 253–265, doi:10.1111/jnc.13536.
26. Yuan, Z.; Becker, E. B. E.; Merlo, P.; Yamada, T.; DiBacco, S.; Konishi, Y.; Schaefer, E. M.; Bonni, A. Activation of FOXO1 by Cdk1 in cycling cells and postmitotic neurons. Science 2008, 319, 1665–1668, doi:10.1126/science.1152337.
27. Yu, C.-H.; Davidson, S.; Harapas, C. R.; Hilton, J. B.; Mlodzianoski, M. J.; Laohamonthonkul, P.; Louis, C.; Low, R. R. J.; Moecking, J.; De Nardo, D.; Balka, K. R.; Calleja, D. J.; Moghaddas, F.; Ni, E.; McLean, C. A.; Samson, A. L.; Tyebji, S.; Tonkin, C. J.; Bye, C. R.; Turner, B. J.; Pepin, G.; Gantier, M. P.; Rogers, K. L.; McArthur, K.; Crouch, P. J.; Masters, S. L. TDP-43 Triggers Mitochondrial DNA Release via mPTP to Activate cGAS/STING in ALS. Cell 2020, 183, 636–649.e18, doi:10.1016/j.cell.2020.09.020.
28. Heslop, K. A.; Rovini, A.; Hunt, E. G.; Fang, D.; Morris, M. E.; Christie, C. F.; Gooz, M. B.; DeHart, D. N.; Dang, Y.; Lemasters, J. J.; Maldonado, E. N. JNK activation and translocation to mitochondria mediates mitochondrial dysfunction and cell death induced by VDAC opening and sorafenib in hepatocarcinoma cells. Biochem. Pharmacol. 2020, 171, 113728, doi:10.1016/j.bcp.2019.113728.

Preprints (www.preprints.org) | NOT PEER-REVIEWED | Posted: 9 July 2021 doi:10.20944/preprints202107.0212.v1

29. Liu, H.; Deng, X.; Shyu, Y. J.; Li, J. J.; Taparowsky, E. J.; Hu, C.-D. Mutual regulation of c-Jun and ATF2 by transcriptional activation and subcellular localization. EMBO J. 2006, 25, 1058–1069, doi:10.1038/sj.emboj.7601020.
30. Del Boca, M.; Caputto, B. L.; Maggio, B.; Borioli, G. A. c-Jun interacts with phospholipids and c-Fos at the interface. J. Colloid Interface Sci. 2005, 287, 80–84, doi:10.1016/j.jcis.2005.01.069.
31. Haase, M.; Koslowski, R.; Lengnick, A.; Hahn, R.; Wenzel, K. W.; Schuh, D.; Kasper, M.; Müller, M. Cellular distribution of c-Jun and c-Fos in rat lung before and after bleomycin induced injury. Virchows Arch 1997, 431, 441–448, doi:10.1007/s004280050121.
32. Blumberg, A.; Sri Sailaja, B.; Kundaje, A.; Levin, L.; Dadon, S.; Shmorak, S.; Shaulian, E.; Meshorer, E.; Mishmar, D. Transcription factors bind negatively selected sites within human mtDNA genes. Genome Biol. Evol. 2014, 6, 2634–2646, doi:10.1093/gbe/evu210.
33. Albensi, B. C. What Is Nuclear Factor Kappa B (NF-κB) Doing in and to the Mitochondrion? Front. Cell Dev. Biol. 2019, 7, 154, doi:10.3389/fcell.2019.00154.
34. Tomer, D.; Chippalkatti, R.; Mitra, K.; Rikhy, R. ERK regulates mitochondrial membrane potential in fission deficient Drosophila follicle cells during differentiation. Dev. Biol. 2018, 434, 48–62, doi:10.1016/j.ydbio.2017.11.009.
35. Keyes, J.; Ganesan, A.; Molinar-Inglis, O.; Hamidzadeh, A.; Zhang, J.; Ling, M.; Trejo, J.; Levchenko, A.; Zhang, J. Signaling diversity enabled by Rap1-regulated plasma membrane ERK with distinct temporal dynamics. Elife 2020, 9, doi:10.7554/eLife.57410.
36. Rasola, A.; Sciacovelli, M.; Chiara, F.; Pantic, B.; Brusilow, W. S.; Bernardi, P. Activation of mitochondrial ERK protects cancer cells from death through inhibition of the permeability transition. Proc. Natl. Acad. Sci. USA 2010, 107, 726–731, doi:10.1073/pnas.0912742107.
37. Masgras, I.; Ciscato, F.; Brunati, A. M.; Tibaldi, E.; Indraccolo, S.; Curtarello, M.; Chiara, F.; Cannino, G.; Papaleo, E.; Lambrughi, M.; Guzzo, G.; Gambalunga, A.; Pizzi, M.; Guzzardo, V.; Rugge, M.; Vuljan, S. E.; Calabrese, F.; Bernardi, P.; Rasola, A. Absence of Neurofibromin Induces an Oncogenic Metabolic Switch via Mitochondrial ERK-Mediated Phosphorylation of the Chaperone TRAP1. Cell Rep. 2017, 18, 659–672, doi:10.1016/j.celrep.2016.12.056.
38. Ramesh, N.; Pandey, U. B. Autophagy dysregulation in ALS: when protein aggregates get out of hand. Front. Mol. Neurosci. 2017, 10, 263, doi:10.3389/fnmol.2017.00263.
39. Ryan, B. J.; Bengoa-Vergniory, N.; Williamson, M.; Kirkiz, E.; Roberts, R.; Corda, G.; Sloan, M.; Saqlain, S.; Cherubini, M.; Poppinga, J.; Bogtofte, H.; Cioroch, M.; Hester, S.; Wade-Martins, R. REST Protects Dopaminergic Neurons from Mitochondrial and α-Synuclein Oligomer Pathology in an Alpha Synuclein Overexpressing BAC-Transgenic Mouse Model. J. Neurosci. 2021, 41, 3731–3746, doi:10.1523/JNEUROSCI.1478-20.2021.
40. Arnold, E. S.; Ling, S.-C.; Huelga, S. C.; Lagier-Tourenne, C.; Polymenidou, M.; Ditsworth, D.; Kordasiewicz, H. B.; McAlonis-Downes, M.; Platoshyn, O.; Parone, P. A.; Da Cruz, S.; Clutario, K. M.; Swing, D.; Tessarollo, L.; Marsala, M.; Shaw, C. E.; Yeo, G. W.; Cleveland, D. W. ALS-linked TDP-43 mutations produce aberrant RNA splicing and adult-onset motor neuron disease without aggregation or loss of nuclear TDP-43. Proc. Natl. Acad. Sci. USA 2013, 110, E736–45, doi:10.1073/pnas.1222809110.
41. Sreedharan, J.; Blair, I. P.; Tripathi, V. B.; Hu, X.; Vance, C.; Rogelj, B.; Ackerley, S.; Durnall, J. C.; Williams, K. L.; Buratti, E.; Baralle, F.; de Belleroche, J.; Mitchell, J. D.; Leigh, P. N.; Al-Chalabi, A.; Miller, C. C.; Nicholson, G.; Shaw, C. E. TDP-43 mutations in familial and sporadic amyotrophic lateral sclerosis. Science 2008, 319, 1668–1672, doi:10.1126/science.1154584.
42. Cacabelos, D.; Ayala, V.; Ramírez-Nunez, O.; Granado-Serrano, A. B.; Boada, J.; Serrano, J. C. E.; Cabré, R.; Nadal-Rey, G.; Bellmunt, M. J.; Ferrer, I.; Pamplona, R.; Portero-Otin, M. Dietary lipid unsaturation influences survival and oxidative modifications of an amyotrophic lateral sclerosis model in a gender-specific manner. Neuromolecul. Med. 2014, 16, 669–685, doi:10.1007/s12017-014-8317-7.
43. Pera, M.; Larrea, D.; Guardia-Laguarta, C.; Montesinos, J.; Velasco, K. R.; Agrawal, R. R.; Xu, Y.; Chan, R. B.; Di Paolo, G.; Mehler, M. F.; Perumal, G. S.; Macaluso, F. P.; Freyberg, Z. Z.; Acin-Perez, R.; Enriquez, J. A.; Schon, E. A.; Area-Gomez, E. Increased localization of APP-C99 in mitochondria-associated ER membranes causes mitochondrial dysfunction in Alzheimer disease. EMBO J. 2017, 36, 3356–3371, doi:10.15252/embj.201796797.
44. McQuin, C.; Goodman, A.; Chernyshev, V.; Kamentsky, L.; Cimini, B. A.; Karhohs, K. W.; Doan, M.; Ding, L.; Rafelski, S. M.; Thirstrup, D.; Wiegraebe, W.; Singh, S.; Becker, T.; Caicedo, J. C.; Carpenter, A. E. CellProfiler 3.0: Next-generation image processing for biology. PLoS Biol. 2018, 16, e2005970, doi:10.1371/journal.pbio.2005970.